ELSEVIER

Computational Materials Science 28 (2003) 518–528

COMPUTATIONAL MATERIALS SCIENCE

www.elsevier.com/locate/commatsci

Simulation of elasto-plastic behaviour of an artificial 3D-structure under dynamic loading

V. Romanova [a,*], R. Balokhonov [a], P. Makarov [a], S. Schmauder [b], E. Soppa [b]

[a] *Institute of Strength Physics and Materials Science, SB RAS, pr.Academicheskii 2/1, Tomsk 634021, Russia*
[b] *Staatliche Materialprüfungsanstalt (MPA), University of Stuttgart, Pfaffenwaldring 32, 70569 Stuttgart, Germany*

Abstract

From the meso-mechanical point of view, the internal structure of a material considerably influences its plastic deformation pattern at the meso-scale level. 2D calculations have shown that the consideration of an internal structure in an explicit form allows us to describe some experimentally observed phenomena, such as plastic strain localisation, material fragmentation, shear and rotation of grain conglomerates, etc. Real structural effects are three-dimensional by nature and in many cases can not be simulated in the framework of a 2D model. It is, therefore, a challenge to perform 3D-modelling for meso-volume behaviour under loading, taking into account material internal structure, and to investigate the phenomena caused by structural effects. In this paper, a special routine to generate a 3D heterogeneous structure is proposed. To calculate a 3D polycrystalline test-piece under plane shock wave as an example, we solve a dynamic problem and obtain numerical solutions using the finite-difference method. The results of 3D simulations are analysed and compared with those for a 2D set.

Keywords: Computational mechanics; 3D-microstructure; Elastic–plastic behaviour; Dynamic loading

1. Introduction

From the viewpoint of modern mechanics and physics of solids [1–6], the internal structure of a material under deformation exerts a predominating influence on the elastic–plastic behaviour at the meso-scale level. Experimental and theoretical investigations [1–7] indicate a key role of internal heterogeneity for the development of stress concentrations and plastic strain localisations under loading.

Although some recent experimental studies, e.g. [8], can give information on the deformation fields inside inhomogeneous metallic materials, the majority of the experimental methods of in situ investigations of plastically deformed materials are mostly reduced to surface observations [1–3,5,7]. In this connection, a numerical simulation including the consideration of an internal structure in an explicit form shows promise for studying plastic deformation patterns in the bulk of heterogeneous media.

The main idea is to introduce an internal structure into the material region for which the calculation is performed by prescribing appropriate physical properties to computational cells

* Corresponding author. Tel.: +7-3822-286876; fax: +7-3822-259576.
E-mail address: varvara@ms.tsc.ru (V. Romanova).

0927-0256/$ - see front matter © 2003 Elsevier B.V. All rights reserved.
doi:10.1016/j.commatsci.2003.08.009

corresponding to different structural elements. The term "computational cells" refers to the elements of a discretized computational area whose geometrical parameters depend on a numerical method to be applied as the next step in calculating response of this structure to loading. The choice of the numerical technique is mainly dictated by the problem to be solved and the material properties. For instance, the method of movable cellular automata (MCA) [9] is mostly useful in calculating brittle and granular media, while elastic–plastic behaviour under dynamic and quasi-static loading is successfully calculated by grid methods such as the finite-element method (FEM) [10], finite-difference approximation (FDA) [11], variational [12] and other techniques.

Except for the simplest geometrical shape (e.g. spherical), the explicit calculations of an internal structure have been mainly performed in a 2D formulation. This fact has been attributed to both the extra complexity of the 3D mechanical problem and the requirements to power characteristics of computing facilities, more stringent in view of complex 3D models. Note that the 2D-simulation of heterogeneous structures has given a considerable impetus to describing and understanding some elasto-plastic phenomena [1,3–6] not addressed before, such as local stress concentrations and relaxations, plastic strain localisations, etc., even though the 3D effects were beyond this study. With the availability of increasingly more powerful hardware, it has recently become feasible to extend this structural approach to the three-dimensional case.

In this connection, the subject of this paper is to design a computer algorithm to generate an artificial 3D-structure and to calculate a 3D polycrystalline test-piece subjected to deformation in a plane shock wave as an example. A simple approach we developed to design artificial 3D-structures is given in Section 2 for a general case. A procedure for designing polycrystalline structures is presented as an example. Mathematical formulation of the three-dimensional problem of dynamic loading is given in Section 3. In Section 4, the elasto-plastic behaviour of the artificial polycrystalline structure under dynamic loading is calculated by the finite-difference method [11]. The 3D numerical results are analysed and compared to those calculated with the 2D model.

2. Computer simulation of artificial 3D-structures

The design of a 3D-structure filling a finite volume with irregularly shaped elements without gaps and overlapping is a topical problem of modern computational mechanics. Over the recent years, several techniques for computer simulation of heterogeneous structures have been developed, including the Monte Carlo Potts models [13], vertex tracking [14], front tracking [15], Voronoi tessellation [16], cellular automata [17] and phase-field approaches [18]. Some of them use a geometrical procedure to generate irregular structures [14–17] and others are based on certain physical principles and thermo-dynamic formulations [13,18]. All of these were originally applied in two dimensions to simulate a polycrystalline structure filling a finite area and their main goal was to obtain reasonable conclusions regarding the kinetic and topological aspects of a 2D grain growth. Although in a few recent works some of these methods were successfully applied to the 3D case, realisation of these techniques in three dimensions is for the most part a non-trivial task calling for optimisation of computational algorithms, since the memory and processing time requirements needed to perform the simulation increase dramatically with the number of spatial dimensions.

In this section, we develop an approach to design a 3D-structure whose mechanical behaviour will be further numerically calculated. Note that it is aimed at describing an artificial rather than real microstructure. The algorithm of filling a finite 3D-volume with artificial structural elements is based on a simple geometrical procedure outlined below.

In the general case, the design of an artificial 3D-structure includes the following steps.

- Setting the geometrical parameters and discretizing the volume to be filled with structural elements.

As the first step, the volume to be filled with structural elements is discretized and three-dimensional coordinates are defined for each discrete

point. Since the design of a 3D-structure precedes the task of simulating its mechanical behaviour, the volume geometry is defined from the conditions of an appropriate mechanical problem and the discretization parameters are dictated by the numerical method to be further applied. In general case, an arbitrarily-shaped test-piece can be descritized by a regular or irregular computational grid and then filled with structural elements.

• Assigning the nucleation centres and defining the law controlling the structural element growth.

Initially, each cell of the discretized volume is assigned a so-called structural index (SI), which reflects that this point belongs to a certain structural element. All points at this stage possess the same SI equal to zero, which implies an initial homogeneity throughout the volume. At the next step, some cells are assigned specific structural indices different from zero. In such a way, they are treated as nucleating centres (NCs) of new structural elements.

Generally, the law of NCs distribution over the discrete cells could be derived from the analysis of experimental data. For instance, when a polycrystalline structure is to be designed for a specific material, the law of NCs distribution over the bulk could be based on the analysis of statistical data on distribution of the impurities that act as crystallization centres in melting. When simulating some composite structures, the law can be obtained from the experimental investigation of distribution of inclusions over the resulting material, provided that the initial relation between volume fractions of the inclusions and the matrix producing remains the same during the material manufacturing process.

In the same way, a law controlling the growth of structural elements can be derived from the experimental evidence. This does not imply that we calculate or just simulate the process of building a structure based on the physical or thermo-dynamical laws, but rather develop an algorithmic procedure from the analysis of a real structure for an artificial structure to be designed with the similar topological characteristics. Note that each kind of structure requires a special consideration since it is obviously not possible to develop a unified law suitable to design a structure of any sort.

• Designing a 3D-structure.

Finally, the volume under consideration is filled with the structural elements in a step-by-step fashion controlled by the following algorithm. At each step in the processing time, the volumes surrounding the nucleating centres are incremented by preset values in accordance with the law of growth. In the general case, the form of the law as well as the increments controlling the growth rate can vary for the different structural elements.

After the volumes of structural elements have been incremented, for each computational cell with a zero SI so far belonging to none of the structural elements it is checked whether its coordinates fall within any of the volumes. If so, the cell is considered to belong to this structural element and its SI is assigned an appropriate value different from zero. Otherwise it retains the zero SI and is checked again at the next step of the processing time. Such a procedure is repeated until the volume fraction of the growing structural elements has reached the preset magnitude. The case of 100% filling means that there are no cells with a zero SI in the computational volume.

As an example let us consider the outlined approach as applied to an idealized case of designing an artificial polycrystalline structure. The test-piece under filling was taken as a right-angled volume discretized by a regular grid. NCs of different sorts were randomly distributed over the volume using the random number generator commonly used in programming. The appropriate nodes were assigned structural indices randomly varied from 1 to the number of NCs. For the sake of simplicity, it was assumed that the growth of all structural elements obeyed the same law, according to which each volume surrounding appropriate nucleating centre increments as spherically-shaped, and the growth rate was assumed to be uniform as well.

The radius of the ith structural element takes an increment dr_i so that $R_i^{n+1} = R_i^n + dr_i$, where R_i^n and R_i^{n+1} are the radii at the n and the $(n+1)$th time steps, respectively. The grid cells with the zero SI are sequentially checked for filling the ith volume. The condition for the jth cell to belong to the ith structural element in the case under consideration takes the form

$$(X_j - X_i)^2 + (Y_j - Y_i)^2 + (Z_j - Z_i)^2 \leqslant R_i^2, \qquad (1)$$

where X_j, Y_j, Z_j and X_i, Y_i, Z_i are the coordinates of the jth cell and the ith nucleating centre, correspondingly. At each step in time, j varies from 1 to the number of NCs and for every its value the index j runs over all cells with the zero SI. The structural index of the jth cell takes the same value as that of the ith structural element, provided that the cell satisfies Eq. (1).

Presented in Fig. 1 are the artificial structures generated by means of the sited procedure under different initial conditions. The input parameters for designing these structures are given in Table 1.

It should be noted that the resulting structural elements deviate widely from a spherical shape despite the fact that all of them were grown in the same manner and at the same rate. Such an irregularity mainly resulted from the non-uniform distribution of the nucleating centres over the initial volume.

The grain size frequency counts corresponding to the structures of 100 and 300 grains are plotted in Fig. 2 as a function of the normalized grain size $V^g/\langle V^g\rangle$, where V^g is the actual grain volume and the angle brackets denote the average grain volume. The grain size distributions are closely approximated by a log-normal fit similar to those obtained from 3D grain-growth models described elsewhere [18]. A comparison of the calculated distributions with the experimental data for steel [19] indicates a reasonable qualitative agreement as well.

Table 1
Characteristics of the artificial 3D-structures presented in Fig. 1

Figure	1a	1b
Grid size	$100\times50\times50$	$100\times100\times100$
Number of NCs	100	300
Number of NCs sorts	42	95

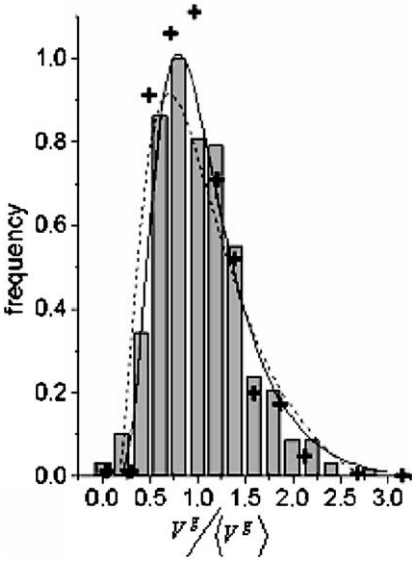

Fig. 2. Grain-size distribution in 3D-simulations of artificial polycrystalline structures. Histogram and log-normal fit corresponding to Fig. 1a (solid-line), log-normal fit corresponding to Fig. 1b (broken line), and experimental data for steel (marked by "+") [18].

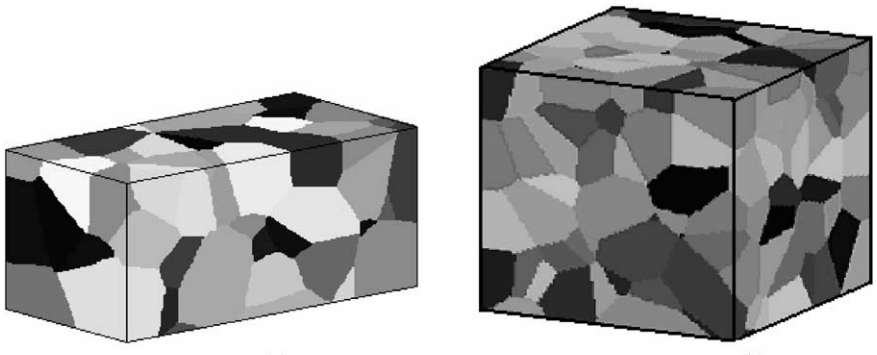

Fig. 1. 3D-design of artificial polycrystalline structures.

3. Mathematical formulation of the three-dimensional problem of dynamic loading

Assuming that a medium under plastic deformation retains its continuity at the meso- and macroscale levels, we apply mathematical tools and a numerical method of continuum mechanics [11]. A system of differential equations in terms of barotropic medium includes the equation of continuity

$$\frac{\dot{V}}{V} - U_{i,i} = 0 \tag{2}$$

the equation of motion

$$\rho \dot{U}_i = \sigma_{ij,j}, \tag{3}$$

and the expression for stress tensor components

$$\sigma_{ij} = -P\delta_{ij} + S_{ij}, \tag{4}$$

where $i = 1, 2, 3$, $j = 1, 2, 3$; $U_i = \dot{x}_i$, U_i and x_i are the velocity vector components and Cartesian coordinates, respectively; $V = \frac{\rho_0}{\rho}$ is the relative volume, and ρ_0 and ρ are the reference and current densities. The upper dot denotes a time derivative.

The pressure was defined from the barotropic equation

$$P = A\left(\frac{\rho}{\rho_0} - 1\right) + B\left(\frac{\rho}{\rho_0} - 1\right)^2 + C\left(\frac{\rho}{\rho_0} - 1\right)^3. \tag{5}$$

The deviatoric stresses are given by the Prandtl–Reuss model for elasto-plastic media

$$\dot{S}^*_{ij} + \lambda S_{ij} = 2\mu\left(\dot{\varepsilon}_{ij} - \frac{1}{3}\dot{\varepsilon}_{kk}\delta_{ij}\right), \tag{6}$$

where μ is the shear modulus. The strain rate tensor is

$$\dot{\varepsilon}_{ij} = \frac{1}{2}(U_{i,j} + U_{j,i}). \tag{7}$$

To eliminate an increase in stress due to rigid rotations of medium elements, we define deviatoric stresses through the Jaumann derivative

$$\dot{S}^*_{ij} = \dot{S}_{ij} - S_{ik}\omega_{jk} - S_{jk}\omega_{ik}, \tag{8}$$

where $\omega_{ij} = \frac{1}{2}(U_{i,j} - U_{j,i})$ is the material spin tensor.

The plastic behaviour is controlled by the von Mises yield criterion, according to which

$$\frac{1}{\sqrt{2}}\sqrt{S_{ij}S_{ij}} = Y_0, \tag{9}$$

where Y_0 is the material yield point. Under plastic yielding, the deviatoric stresses are corrected by multiplying by the term $\frac{Y_0}{\sqrt{3S_{ij}S_{ij}}}$.

The parameter λ in (6) has the meaning of the power of plastic deformation energy

$$\lambda = \frac{3\mu}{Y_0^2} S_{ij}\left(\dot{\varepsilon}_{ij} - \frac{1}{3}\dot{\varepsilon}_{kk}\delta_{ij}\right). \tag{10}$$

$\lambda \equiv 0$ under elastic deformation, and $\lambda > 0$, provided that Eq. (9) is fulfilled.

The system of Eqs. (2)–(10) was numerically solved by the finite difference method [11,20] for a cubic discretized grid. The partial differential equations are discretized in 3D space and time, so that coordinates x_i and velocities U_i correspond to the nodes, while the stress and strain tensor components, volume and density are related to the cells. The node velocities and strain rate tensor components are calculated at an intermediate time with the $n + 1/2$ index, and the remaining values are defined at the $n, n + 1, \ldots$ time indices.

To dump oscillations behind the shock wave front caused by the numerical method itself, we add artificial viscosity terms to the stress tensor components

$$\sigma_{ij} = -(P + Q)\delta_{ij} + (S_{ij} + q_{ij}), \tag{11}$$

$$q_{ij} = \mu_1\left(\dot{\varepsilon}_{ij} - \frac{1}{3}\frac{\dot{V}}{V}\delta_{ij}\right) + \mu_1\dot{\varepsilon}_{ij}\delta_{ij}, \tag{12}$$

$$Q = \begin{cases} 0, & \dot{V}/V \geqslant 0, \\ C_0\rho\left(h\frac{\dot{V}}{V}\right)^2 + C^*C_l\rho h\left|\frac{\dot{V}}{V}\right|, & \dot{V}/V < 0. \end{cases} \tag{13}$$

Here $\mu_1 = a_1\rho_0 C_l h/V$; C_0, C^* and a_1 are the modelling parameters; C_l is the sound velocity; h is the minimum space between the computational grid nodes. Note, that under the finite-difference approximation σ_{ij}, S_{ij} and P correspond to the $n + 1$ time index and Q and q_{ij} are calculated from the $n + 1/2$ step in time.

The 3D calculation has been performed for a polycrystalline aluminium test-piece under a plane

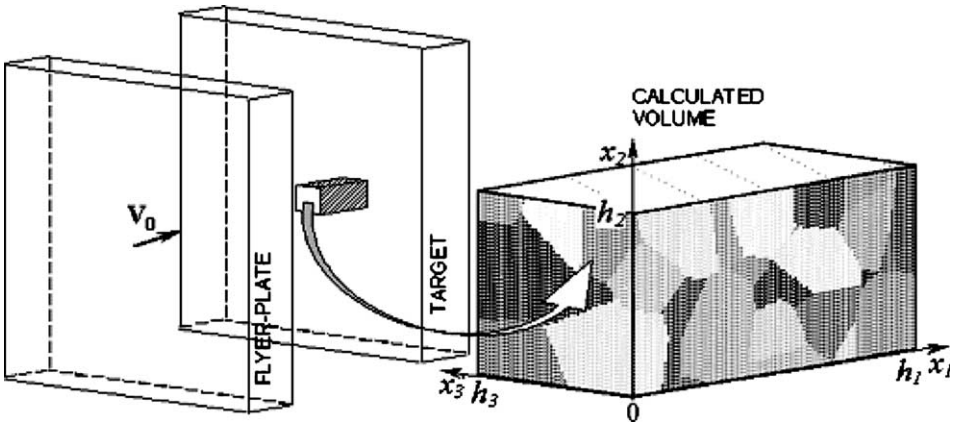

Fig. 3. Schematic illustration of the flyer-plate test and the polycrystalline volume. Arrow points to an enlarged 3D computational grid.

shock wave. The artificial structure calculated is shown in Figs. 1(a) and 3. Differently-coloured grains were distinguished by their yield stresses:

$$Y_0^i = \langle Y_0 \rangle + \langle Y_0 \rangle \frac{0.15 \cdot (N_{\text{ph}} - 2i)}{N_{\text{ph}}}, \tag{14}$$

where $\langle Y_0 \rangle$ is the average dynamic yield point, N_{ph} is the number of NCs sorts, and index i varies from 1 to N_{ph}. Referring to the structure image, the darker the grain colour, the lower its yield stress.

The structure parameters is given in Table 1. Material constants and modelling parameters are presented in Table 2. The spatial step of the reference computational grid was 5×10^{-4} cm along all three dimensions.

Considering the plane shock wave, we disregarded the unloading waves from consideration to be able to arrive from the side surfaces of the target. Referring to Fig. 3, the boundary conditions were given in the form

Table 2
Material and modelling parameters

Parameter	Value	Parameter	Value
ρ_0, g/cm^3	2.7	$\langle Y_0 \rangle$, Gpa	0.346
μ, GPa	27.7	C_l, cm/μs	0.634
A, GPa	76.5	C^*	0.5
B, GPa	165.9	C_0	2
C, GPa	42.8	a_1	0.037

$$\begin{aligned}
&\sigma_{ij}(h_1, x_2, x_3, t) = 0,\\
&U_i(x_1, x_2, 0, t) = U_i(x_1, x_2, h_3, t)\\
&\qquad = U_i(x_1, 0, x_3, t)\\
&\qquad = U_i(x_1, h_2, x_3, t)\\
&\qquad = U_i(0, x_2, x_3, t) = 0
\end{aligned} \tag{15}$$

where $i = 2,\ 3$; h_1, h_2 and h_3 are the test-piece lengths along the x_1, x_2 and x_3 directions, respectively.

At $t = 0$, a shock wave front was specified at the surface $x_1 = 0$ as a jump in the normal component U_1 of the velocity vector. Under further calculation, the amplitude of U_1 at the surface nodes was kept constant to avoid the unloading effects:

$$U_1(0, x_2, x_3, t) = V_0, \tag{16}$$

where $V_0 = 500$ m/s.

On the surfaces $x_2 = 0$, $x_2 = h_2$, $x_3 = 0$ and $x_3 = h_3$ the component U_1 of the velocity vector was defined from a finite-difference approximation of the equation of motion as suggested in [11] for a boundary fixed along x_2 and x_3 directions, whereas tangential components U_2 and U_3 on these surfaces were equal to 0.

It should be marked that the boundary conditions in such a form are realistic, provided that the unloading waves propagating from the target sides do not reach the volume under study during the calculation time.

4. Calculation results

In our earlier works [6,21–23], we have made 2D numerical simulations of the elasto-plastic behaviour of a polycrystalline material subjected to high-rate deformation in weak shock waves. Structural characteristics such as grain size and shape as well as loading conditions, including the shock wave amplitude and the geometry of the flyer-plate—target arrangement, were varied in the calculations to comprehensively investigate their effects on elasto-plastic behaviour. The results allowed us to reveal some intriguing phenomena of plastic strain localisation and development, attributed to both structural heterogeneity and specific stress–strain state realized due to compression in a plane shock wave.

Though intuition suggests that the results obtained in [6,21–23] could be at least qualitatively extended to the 3D-case, providing similar patterns of elasto-plastic deformation in the bulk of material, additional calculations are required to prove or disprove this assumption and delineate the frames of its validity. So this paper is projected to give the beginning of a series of computational studies devoted to investigations of stress–strain features in 2D and 3D formulations.

To begin with, we have performed simulations for the polycrystalline test-piece (Fig. 1a) subjected to deformation in the plane shock wave as schematically illustrated in Fig. 3.

Note that in the 3D case, along with the complexity of the computational procedure, visualisation and analysis of the calculation results also become more difficult. Due to its heterogeneity, every layer of the test-piece exhibits an individual stress–strain pattern that, in addition, evolves in time. In this section we, therefore, give only two representative illustrations of deformation patterns and velocity vector fields on cutting-planes oriented perpendicular (Figs. 4 and 5) and parallel (Fig. 6) to the shock wave front, with the conclusions drawn for the general case.

Fig. 4 shows the results of a 3D-calculation compared with those obtained in 2D-modelling of plane strain conditions. The grain structure in the 2D model is identical to that in the cross-section shown for the 3D model. Note, however, that in the 2D case of plane strain the structure corresponds to the infinitely long columnar grains oriented in the x_3 direction.

The velocity vector deviation from the fields calculated for a homogeneous medium are depicted in Fig. 4. These vector fields indicate a deviation of the particle motion from a rectilinear motion in the direction of wave propagation. It is evident, the deviation of particle motion from a rectilinear trajectory is caused by the difference in the yielding characteristics of adjacent grains.

As the figures show, the 2D and 3D vector fields are qualitatively comparable if not identical to a certain extent, whereas a quantitative comparison demonstrates some differences. The "vortices" mainly develop near the triple point zones of grains markedly differing in their yield characteristics. However, in the 3D simulation the velocity vectors within the volume have three non-zero components as distinct from the 2D case of plane strain when U_3 is equal to 0. That is why the plane projections of the velocity vectors in the 3D simulation are shorter than those in the 2D model. In other words, under the plane strain conditions the ability of the material particles to deviate from the direction of wave propagation is confined within the only plane. In the 3D simulation the additional degrees of freedom can apparently result in a development of structural-accommodation modes other than those evolving under the plane strain.

The deformation images in Fig. 4 indicate that the resulting patterns of plastic strain localisation are quite similar qualitatively. The plastic strain localises mainly along the interfaces oriented in the direction of maximum tangential stresses. The plastic strain gradients are more pronounced near the boundaries between the grains exhibiting a high difference in their yield characteristics. It is worth noting that all the bands of localised deformation displayed in the images as lighter lines border darker zones indicating lower strain. The development of plastic deformation along the boundaries with higher ability to yielding results in unloading and stress relaxation in the adjacent sub-boundary zones of neighbouring grains.

A 3D simulation proved to be a useful tool for investigating the deformation modes developing in a cross-section parallel to the shock wave front,

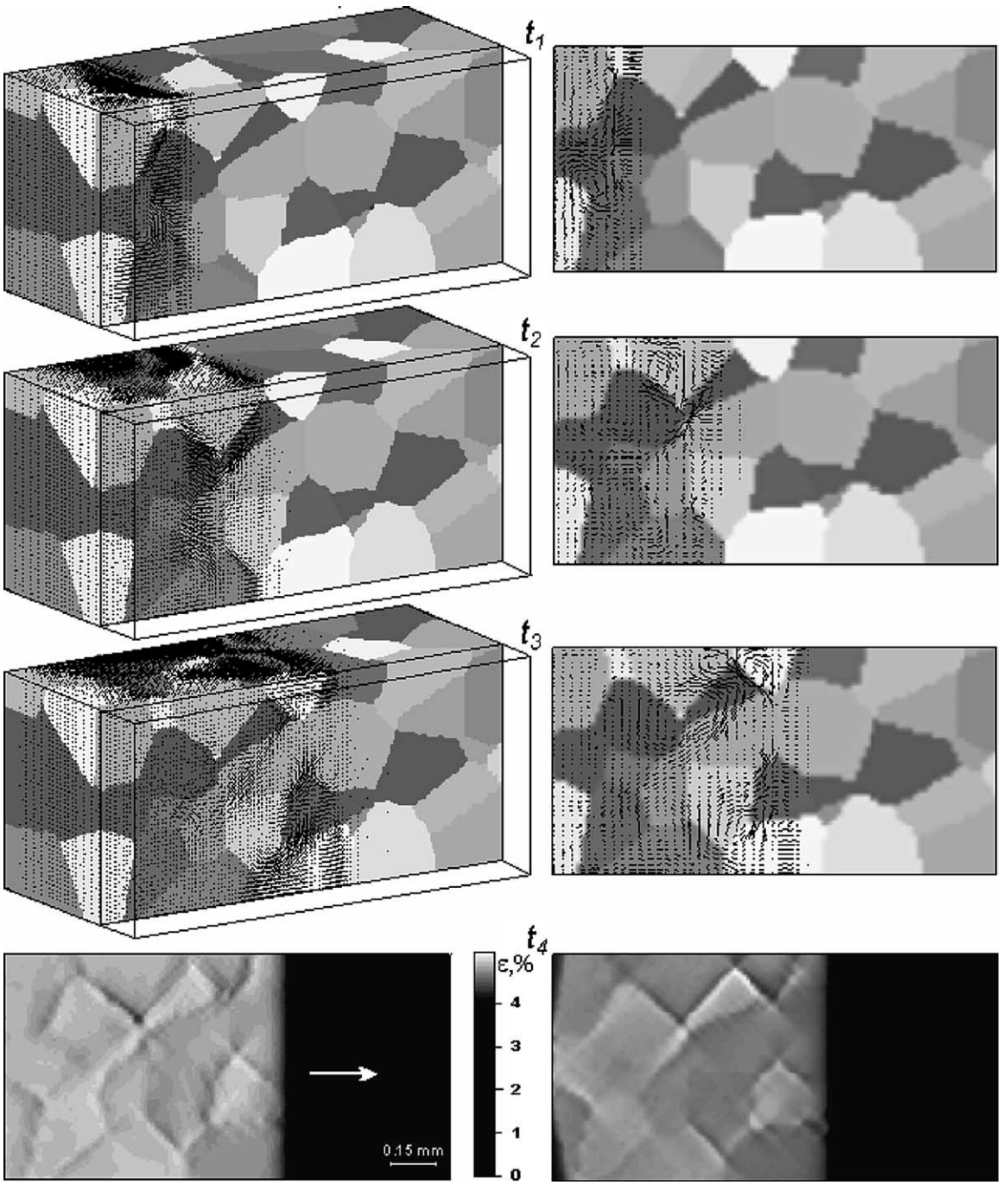

Fig. 4. Simulations of polycrystal behaviour under the plane shock wave in three (left) and two (right) dimensional sets: deviation of velocity vectors from those obtained for a homogeneous medium (three upper rows) and equivalent plastic strains (lower plots) in the cross-section $x_3 = 0.0075$ cm (refer to the schematic in Fig. 3). Times, μs: $t_1 = 0.014$, $t_2 = 0.028$, $t_3 = 0.042$, and $t_4 = 0.056$.

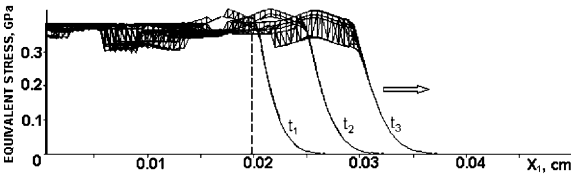

Fig. 5. 3D-simulation of polycrystal behaviour under a plane shock wave: evolution of equivalent stresses plotted as projections on the x_1x_2-plane; time, μs: $t_1 = 0.028$, $t_2 = 0.035$, and $t_3 = 0.042$.

which was impossible in the 2D formulation of the problem. Plotted in Fig. 5 as projections on x_1x_2-plane are the profiles of equivalent stresses, corresponding to different moments of time. The average value of the stresses behind the front is equal to $\langle Y_0 \rangle$ (see Table 2) and deviation from this value to about 15% corresponds to the yield points preset by Eq. (14). Presented in Fig. 6 are the velocity vector fields and plastic deformation pattern in the cross-section parallel to the shock wave front.

Considering Figs. 5 and 6 together we can make the following conclusions. At the beginning of the plastic front (see Figs. 5 and 6, t_1) the deviation of velocity vectors from the direction of wave prop-

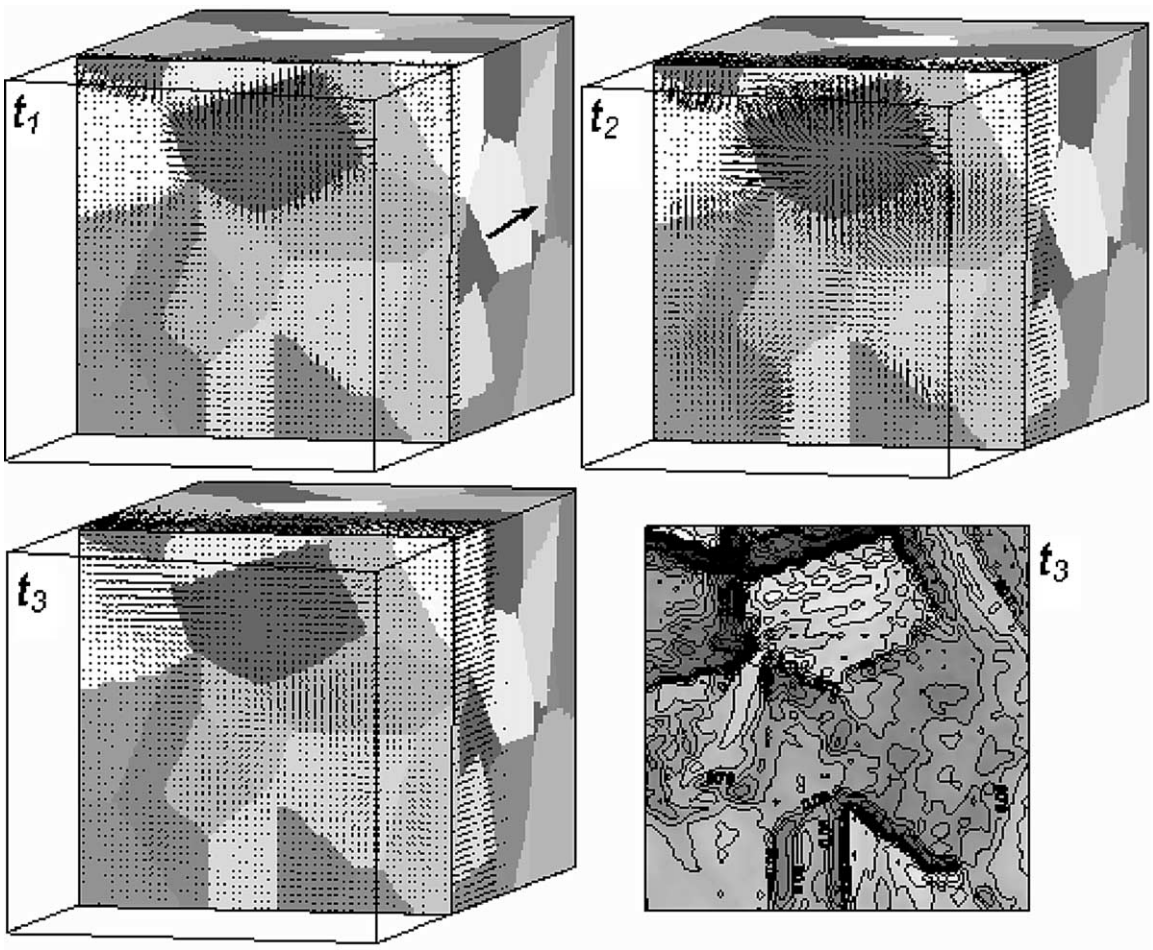

Fig. 6. 3D-simulation of polycrystal behaviour under a plane shock wave: deviation of velocity vectors from those obtained for a homogeneous medium and equivalent plastic strains in the cross-section $x_1 = 0.02$ cm (marked by dashed line in Fig. 5); t_1, t_2 and t_3 are the same as those in Fig. 5.

agation manifests itself at first near the grain boundaries. As plastic front passes through the cross-section (Figs. 5 and 6, t_2) the velocity field indicates the higher the grain deformability, the stronger the non-uniform motion it is involved into. A correlation between the stress-profile and velocity field corresponding to t_3 shows that the non-uniform motion is mainly exhibited in the area of stress gradients that becomes practically uniform in the region of stress plateau behind the front. This fact agrees with the earlier assumption [21] that the stress–strain gradients in a shock wave front are a primary reason for origination of bands of localised plastic deformation.

As in the previous case of a cutting-plane oriented parallel to the wave direction, the plastic deformation pattern presented in Fig. 6 by the image and contour lines demonstrates higher strain gradients in the vicinity of boundaries between grains with different ability for yielding.

5. Conclusions

In this paper, a meso-mechanical approach to simulate the elasto-plastic behaviour of heterogeneous media with explicit consideration for the material structure has been extended to the three-dimensional case. To do so, we have developed a computational procedure to design artificial 3D structures filling a finite volume with irregularly shaped elements. The algorithm outlined for the general case has been applied to design artificial polycrystalline structures.

As the next step, we have performed 3D-simulations of elasto-plastic behaviour of a polycrystalline aluminium alloy under a plane shock wave. The results of the 3D-calculation have been analysed and compared with those obtained from the 2D-approximation. It has been shown that the 2D and 3D deformation patterns are comparable within a certain degree.

It should be marked, however, that the outlined conclusions hold for the specific case of deformation under a plane shock wave of a certain amplitude without unloading effects. It could hardly be extended to the case of other loading conditions without certain proofs calling for special calculations. Thus, with this paper we plan to start a set of computational studies devoted to investigations of stress–strain features in the case of a 3D heterogeneous structure under different types of loading.

Acknowledgements

Support of the Deutscher Akademischer Austauschdienst (DAAD) through the project A0206390/REF.325 is gratefully acknowledged.

References

[1] V.E. Panin (Ed.), Physical mesomechanics of heterogeneous media and computer-aided design of materials, Cambridge International Science Publishing, Cambridge, 1998.
[2] V.E. Panin, Foundations of physical mesomechanics, Phys. Mesomech. 1 (1998) 5–22.
[3] R. Pyrz, J. Schjødt-Thomsen, J.C. Rauhe, T. Thomsen, L.R. Jensen (Eds.), Int. Conference on New Challenges in Mesomechanics, Aalborg University, Denmark, August 26–30, 2002.
[4] P.V. Makarov, V.A. Romanova, Mesoscale plastic flow generation and development for polycrystals, Theor. Appl. Frac. Mech. 33 (2000) 1–7.
[5] E. Soppa, S. Schmauder, G. Fischer, J. Thesing, R. Ritter, Influence of the microstructure on the deformation behaviour of metal–matrix composites, Comput. Mater. Sci. 16 (1999) 323–332.
[6] P.V. Makarov, S. Schmauder, O.I. Cherepanov, I.Yu. Smolin, V.A. Romanova, R.R. Balokhonov, D.Yu. Saraev, E. Soppa, P. Kizler, G. Fischer, S. Hu, M. Ludwig, Simulation of elastic plastic deformation and fracture of materials at micro-, meso- and macro-levels, Theor. Appl. Frac. Mech. 37 (2001) 183–244.
[7] S. Toyooka, R. Widiastuti, Q. Zhang, H. Kato, Dynamic observation of localized pulsation generated in the plastic deformation process by electronic speckle pattern interferometry, Jpn. Appl. Phys. 40 (2001) 873–876.
[8] J.-Y. Buffière, E. Maire, P. Cloetens, G. Lormand, R. Fougères, Characterization of internal damage in a MMC_p using X-ray synchrotron phase contrast micro-tomography, Acta Mater. 47 (1999) 1613–1625.
[9] S.G. Psakhie, G. Ostermeyer, A.I. Dmitriev, E.V. Shilko, A.Yu. Smolin, S.Yu. Korostelev, Method of movable cellular automata as a new trend of discrete computational mechanics. I. Theoretical description, Phys. Mesomech. 2 (2000) 5–12.

[10] R.J. Astley, Finite Elements in Solids and Structures, The University Press, Cambridge, 1992.
[11] M.L. Wilkins, M.W. Guinan, Plane stress calculations with a two dimensional elastic–plastic computer program, UCRL-77251, University of California, Lawrence Livermore Laboratory, 1976.
[12] O.I. Cherepanov, Numerical simulation of plastic behaviour of materials allowing for descending branch of stress–strain diagram, Phys. Mesomech. 1–2 (1999) 5–16.
[13] M.P. Anderson, D.J. Srolovitz, G.S. Crest, P.S. Sahni, Monte Carlo simulation of grain growth in textured metals, Acta Metall. 32 (1984) 783–789.
[14] K. Kawasaki, T. Nagai, K. Nakashima, Vertex models for two-dimensional grain growth, Philos. Mag. B 60 (1998) 399–407.
[15] H.J. Frost, C.V. Thompson, C.L. Howe, J. Whang, A two-dimensional computer simulation of capillary-driven grain growth: preliminary results, Scripta Metal. Mater. 22 (1988) 65–70.
[16] S. Ghosh, Z. Nowak, K. Lee, Quantitative characterization and modeling of composite microstructures by Voronoi cells, Acta Mater. 45 (1997) 2215–2237.
[17] J. Geiger, A. Roósz, P. Barkóczy, Simulation of grain coarsening in two dimensions by cellular-automaton, Acta Mater. 49 (2001) 623–629.
[18] C.E. Krill, L.-Q. Chen, Computer simulation of 3-D grain growth using a phase-field model, Acta Mater. 50 (2002) 3057–3073.
[19] K. Matsuura, Y. Itoh, T. Ohmi, K. Ishii, Mater. Trans. JIM 35 (1994) 247–253.
[20] B. Alder, S. Fernbach, M. Rotenberg (Eds.), Methods in Computational Physics, vol. 3, Academic Press, New York, 1964.
[21] R.R. Balokhonov, P.V. Makarov, V.A. Romanova, I.Yu. Smolin, Simulation of crystal plasticity under dynamic loading, Comput. Mater. Sci. 16 (1999) 355–361.
[22] V.A. Romanova, R.R. Balokhonov, P.V. Makarov, I.Yu. Smolin, Numerical modeling of the behavior of a relaxing medium with an inhomogeneous structure under dynamic loading, Chem. Phys. Rep. 18 (10–11) (2000) 2191–2203.
[23] R.R. Balokhonov, P.V. Makarov, V.A. Romanova, I.Yu. Smolin, I.V. Savlevich, Numerical modelling of multi-scale shear stability loss in polycrystals under shock wave loading, J. Phys. IV 10 (2000) 515–521.